Heliyon 7 (2021) e06079

Contents lists available at ScienceDirect

Heliyon

journal homepage: www.cell.com/heliyon

Research article

Quantum computational investigations and molecular docking studies on amentoflavone

Márcia M. Marinho [a,*], Francisco Wagner Q. Almeida-Neto [b], Emanuelle M. Marinho [b], Leonardo P. da Silva [b], Ramon R.P.P.B. Menezes [a], Ricardo P. dos Santos [c], Emmanuel S. Marinho [d], Pedro de Lima-Neto [b], Alice M.C. Martins [a]

[a] Departamento de Análises Clínicas e Toxicológicas, Centro de Ciências da Saúde, Universidade Federal do Ceará, Campus Porangabussu, 60430-370, Fortaleza, Ceará, Brazil
[b] Departamento de Química Analítica e Físico-Química, Centro de Ciências, Universidade Federal do Ceará, Campus do Pici, Bloco 940, 60440-900, Fortaleza, Ceará, Brazil
[c] Engenharia de Computação / Biotecnologia, Universidade Federal do Ceará, Campus de Sobral, 62010-560, Sobral Ceará, Brazil
[d] Faculdade de Filosofia Dom Aureliano Matos, Universidade Estadual do Ceará, 62930-000, Limoeiro do Norte, Ceará, Brazil

ARTICLE INFO

Keywords:
Antichagasic agent
Biflavonoid
DFT
Fukui analysis
NLO

ABSTRACT

Chagas disease is a neglected tropical disease caused by the protozoan parasite *Trypanosoma cruzi*, with approximately 6–7 million people infected worldwide, becoming a public health problem in tropical countries, thus generating an increasing demand for the development of more effective drugs, due to the low efficiency of the existing drugs. Aiming at the development of a new antichagasic pharmacological tool, the density functional theory was used to calculate the reactivity descriptors of amentoflavone, a biflavonoid with proven anti-trypanosomal activity in vitro, as well as to perform a study of interactions with the enzyme cruzain, an enzyme key in the evolutionary process of *T-cruzi*. Structural properties (in solvents with different values of dielectric constant), the infrared spectrum, the frontier orbitals, Fukui analysis, thermodynamic properties were the parameters calculated from DFT method with the monomeric structure of the apigenin used for comparison. Furthermore, molecular docking studies were performed to assess the potential use of this biflavonoid as a pharmacological antichagasic tool. The frontier orbitals (HOMO-LUMO) study to find the band gap of compound has been extended to calculate electron affinity, ionization energy, electronegativity electrophilicity index, chemical potential, global chemical hardness and global chemical softness to study the chemical behaviour of compound. The optimized structure was subjected to molecular Docking to characterize the interaction between amentoflavone and cruzain enzyme, a classic pharmacological target for substances with anti-gas activity, where significant interactions were observed with amino acid residues from each one's catalytic sites enzyme. These results suggest that amentoflavone has the potential to interfere with the enzymatic activity of cruzain, thus being an indicative of being a promising antichagasic agent.

1. Introduction

Chagas disease is a tropical disease caused by the protozoan parasite *Trypanosoma cruzi*, classified as neglected by the World Health Organization. The Chagas disease is transmitted to humans by the triatomine insect, popularly known, in Brazil, as the barber [1]. Currently, there are approximately 6–7 million infected people in the world and it is estimated that 70 million people will be able to contract this disease. This is an endemic disease in Latin America, Africa and Asia, but also found in non-endemic developed countries such as Canada, Spain, Japan and Australia [2,3]. Currently, benznidazole and nifurtimox are the only drugs used for the pharmacological treatment of Chagas disease, developed almost fifty years ago, have limited effectiveness in the chronic phase of the disease. However, these drugs led to the occurrence of several side effects, such as polyneuritis, bone marrow depression, lymphoma and dermatitis [4].Therefore, it is necessary to look for new bioactive substances, as well as therapeutic strategies that promote

* Corresponding author.
E-mail address: marinho.marcia@gmail.com (M.M. Marinho).

https://doi.org/10.1016/j.heliyon.2021.e06079
Received 27 October 2020; Received in revised form 1 December 2020; Accepted 20 January 2021

greater selectivity over parasites without causing so many complications to the host.

One of the strategies is the search for substances that inhibit key enzymes, such as cruzain, in order to interrupt the parasite's reproductive cycle [5,6]. In this perspective, the challenger of finding new drugs has been supported by the use of molecular modelling methods, which allow, through mathematical algorithms, to characterize electronic and structural properties of substances which have potential to become a pharmacological tools, as well as how to study the interaction of these molecules with their potential therapeutic targets (molecular Docking) [7,8]. Among the modelling techniques, it can be highlighted the formalism of the functional density theory (DFT), which enables the calculation of physicochemical properties of the investigated molecules at microscopic level, and with good accuracy and low computational cost. For instance, this quantum method make possible to identify the frontier orbitals, nucleophilic and/or electrophilic sites of the molecule, kinetics and thermodynamic descriptors [9,10]. Thus, DFT is a fundamental step for analysing the pharmacological potential and identifying the essential pharmacophore for drug design. In the work of Pan *et al* [11], the amentoflavone molecule was studied using the DFT method with B3LYP at 6-31G(d) basis set, the structural optimization was performed in the gas phase (vacuum) and they characterized only the Frontier Molecular Orbitals and the Mulliken charge distribution by the Molecular Electrostatic Potential. However, thinking about the potential pharmacological use of organic molecule to fight Chagas disease, it is necessary to perform DFT molecular modeling calculations taking in account the dielectric constants of the several solvents in order to generate conformational relevant data to the development of a pharmacological tool, since the investigated molecules will have to be dissolved before being applied to humans.

The Density Functional Theory (DFT) method allows the calculation of the geometric optimization of organic molecules. Furthermore, the infrared (IR) spectra can be simulated, the Frontier Molecular Orbitals (FMO) can be calculated for electronic characterization and to obtain the quantum reactivity descriptors in order to understand the global reaction of the behavior of the molecule as a nucleophile or an electrophile [10]. A local reactivity can also be performed by the Fukui functions since it makes possible the comprehension which atoms contribute most significantly to the molecule's reactivity [9]. The global and local reactivity analysis can relate the molecular biological activity since both allow the identification of the most reactive regions of the molecule for the interaction with the target protein.

Molecular docking is an efficient computational tool in molecular recognition process studies [12]. It simulates the modes of interaction, conformation and orientation, allowing the estimation of the interaction energies between two molecules in three-dimensional space, such as protein-protein and protein-ligand [13], based on two elements, a potential energy function, usually associated with a force field (used to define the binding affinity of the ligand and the receptor) and a search algorithm, which defines the ligand conformational space sampling that determines the minimum global energy for the ligand-receptor complex [13]. It also analyses the affinity of a ligand to a receptor binding site, in which the active conformations of molecules and enzymes exhibit geometric and chemical complementarity, which are essential for the success of therapeutic treatments [14].

To begin the development of new drugs, naturally occurring structures have been used as a starting point, with the molecular skeleton for more than 50% of the new drugs available today [15]. In this context, it can be highlighted the cashew tree (*Anacardium occidentale L.*), native to Brazil, found abundantly in the Northeast biodiversity, where it stands out for its high socioeconomic importance to the region, representing 99.7% of Brazilian cashew exports [16]. Found in the leaf of *Anacardium occidentale L.*, the biflavonoid amentoflavone, stands out for having several biological activities such as leishmanicidal, antitrypanosomal ($IC_{50} > 50\mu M$) [17,18,19], antifungal [20,21] and antioxidant [22]. In addition to its natural occurrence, amentoflavone can be obtained synthetically by oxidative coupling of two apigenin molecules, resulting in a bond between the C-3 positions of the hydroxyphenyl ring and C-8 of the chromene ring, thus enabling its production in large scale (Figure S1-Supplementary material).

In view of the emergency situation of developing new pharmacological tools for the treatment of Chagas disease, this study aimed carry out a DFT in-silico investigation to assess the molecular reactivity descriptors of amentoflavone, a biflavonoid that has proven antitrypanosomal *in vitro* activity, and to perform molecular docking studies to assess the potential use of this biflavonoid as a pharmacological antichagasic tool.

2. Materials and method

2.1. DFT analysis

In the present study, the computational chemistry calculations were done within the scope of Density Functional Theory (DFT), which is one of the most effective way to analyse the stability and reactivity of chemical species. The DFT quantum calculations for the ground state electronic and reactive properties of amentoflavone and apigenin were performed using the Gaussian 09 program [23] and the Gauss View 5 program [24] to drawn the input molecules. The apigenin molecule was optimized so that it became a reference parameter for calculating the electronic and reactive properties of the amentoflavone molecule. Due to the different orbital energies brought by these molecules, a restricted Kohn-Sham functional, together with Becke's [25,26] three parameter functional (B3) [27] for the exchange part and the Lee-Yang-Parr gradient corrected correlation functional (LYP) [28] were applied to bring the optimized geometrical structure. In order to have a secure basis set, a 6–311++G(d,p) [28] polarized base was used. The optimization was also carried out in the gas phase and in several implicit solvents available in the Gaussian 09 program package and using the Integral Equation Formalism – Polarizable Continuum Model (IEF-PCM) solvation model [29] to understand the structural properties of amentoflavone molecule due to the structure of the dimer that allows an angle between the two monomer structure. To ensure the validity of the optimization, a vibrational frequency calculation was done to get the theoretical infrared spectra in methanol as implicit solvent applying the same level of theory. The theoretical assignments were done using the VEDA 4 software [30] with a scaling factor of 0.967 for the computational level used in this work. To obtain the isosurfaces of the Frontier Molecular Orbitals (FMO), the Highest Occupied Molecular Orbital (HOMO) and the Lowest Unoccupied Molecular Orbital (LUMO), it was used the trial version of Chemcraft - graphical software for visualization of quantum chemistry computations version 1.8 software (https://www.chemcraftprog.com). The thermodynamic data, internal energy (U), enthalpy (H), entropy (S) and Gibbs free energy (G), were obtained from the calculation of the vibrational and statistical thermodynamic analysis at 298.15 K and 1 atm at B3LYP/6–311++G(d,p) computational level with methanol as implicit solvent, which was the same condition for the fundamental vibrational frequencies and optimization calculations [31].

The molecular descriptors were calculated at B3LYP/6–311++G(d,p) level of theory to estimate the reactivity of amentoflavone and apigenin from the energy values of the highest occupied molecular orbital (HOMO) and the lowest unoccupied molecular orbital (LUMO) [32,33]. A higher value of energy for the HOMO orbital indicates a reasonable tendency of the chemical species to donate electronic density and a lower value of the energy for the LUMO orbital shows, a propensity to receive electronic density [34]. Therefore, the energy gap (n E_{gap}), defined as the difference of the energies for the LUMO-HOMO orbitals (Eq. 1), shows a direct relationship between the frontier orbitals and chemical reactivity: for large values of n E_{gap} implies lower reactivity and for a short value of n E_{gap}, suggest higher reactivity [35].

$$\Delta E_{gap} = E_{LUMO} - E_{HOMO} \quad (1)$$

Besides the energy gap, there are other quantities also called reactivity descriptors that help computational chemists to predict the behaviour of a chemical species in respect to another. According to DFT-theorem proposed by Koopmans [36], the ionization energy (I) and electron affinity (A) of a chemical compound are related respectively to the energy of the HOMO orbital (Eq. 2) and the energy of the LUMO orbital (Eq. 3).

$$I = -E_{HOMO} \tag{2}$$

$$A = -E_{LUMO} \tag{3}$$

Within the theory of DFT, chemical quantities such as electronegativity (χ), chemical potential (μ) and global chemical hardness (η) can be defined as the derivative of the molecule electronic energy (E) in respect to the number of total electrons (N) at a constant external potential (υ). The mathematical expressions can be seen as follows [37,38,39,40,41].

$$\chi = -\mu = \left(\frac{\partial E}{\partial N}\right)_{\upsilon} \tag{4}$$

$$\eta = \frac{1}{2}\left(\frac{\partial^2 E}{\partial N^2}\right)_{\upsilon} \tag{5}$$

According to the work of Iczkowski and Margrave and the finite differences method [9], the electronegativity and chemical potential can be expressed in the function of the ionization energy and electron affinity (Eq. 6). The global chemical hardness can be estimated using Janak's theorem and the valence state parabola model [42,43](Eq. 7).

$$\chi = -\mu = \frac{I + A}{2} \tag{6}$$

$$\eta = \frac{I - A}{2} \tag{7}$$

The global softness (S) is defined as the inverse of global chemical hardness [44](Eq. 8).

$$S = \frac{1}{\eta} \tag{8}$$

Parr *et al.* [45] introduced the global electrophilicity index (ω) defined as the susceptibility of a chemical species (atom, molecule or ion) to accept electronic density. The higher value of ω implies that the species can be considered a good electrophile. Thus, a good nucleophile is described by lower values of ω. The quantitative expressions of ω is followed by Eq. 9 and Eq. 10. In this sense, nucleophilicity (ε) is defined as the inverse of global electrophilicity index [46](Eq. 11).

$$\omega = \frac{\mu^2}{4\eta} = \frac{\chi^2}{4\eta} \tag{9}$$

$$\omega = \frac{(I + A)^2}{8(I - A)} \tag{10}$$

$$\varepsilon = \frac{1}{\omega} \tag{11}$$

All the reactivity descriptors seen until now are related to the global properties of the chemical species. Fukui [34] proposed local reactivity descriptors called Fukui functions or Fukui index, $f(r)$, which measure the reactive regions and the electrophilic, nucleophilic and radical behaviour of the chemical compounds. Mathematically, the electronic Fukui function is defined as the first order derivative of electronic density $\rho(r)$ with respect to the total number of electrons (N) at a constant external potential $\upsilon(r)$ (Eq. 12) [47].

$$f(r) = \left(\frac{\partial \rho(r)}{\partial N}\right)_{\upsilon} \tag{12}$$

In consequence of the finite differences method [41], the condensed Fukui functions can be expressed, called condensed Fukui functions, as follow for the nucleophilic (f_k^+) (Eq. 13), electrophilic (f_k^-) (Eq. 14) and radical attack (f_k^o) (Eq. 15).

$$f_k^+ = q_k(N+1) - q_k(N) \tag{13}$$

$$f_k^- = q_k(N) - q_k(N-1) \tag{14}$$

$$f_k^o = \frac{q_k(N+1) - q_k(N-1)}{2} \tag{15}$$

Where $q_k(N+1)$, $q_k(N)$ and $q_k(N-1)$ represent the charge value of Hirshfeld population analysis for the k atom for anionic, neutral and cationic species respectively. The condensed Fukui functions can be used together with the electrophilicity index (ω) to estimate local electrophilic or nucleophilic sites using the quantities called dual descriptor defined by Δf (Eq. 16) and multiphilic descriptor described by $\Delta\omega$ (Eq. 17) [48].

$$\Delta f = f_k^+ - f_k^- \tag{16}$$

$$\Delta\omega = \omega\Delta f \tag{17}$$

If $\Delta\omega$ and $\Delta f > 0$, it implies that the reactive site has an electrophilic character, while $\Delta\omega$ and $\Delta f < 0$, it means that the reactive site has nucleophilic character [49,50]. Finally, the molecular electrostatic potential was calculated and plotted using the Gabedit 2.5.0 software [51]. The results related to the electronic Fukui functions, and the dual descriptor were plotted using the VESTA 3 software [52]. The cube files were generated by Multiwfn software [53].

Finally, to expand the study of applicability beyond of the biological use of the amentoflavone, the calculation of the nonlinear optical (NLO) properties, the total dipole moment (μ_{tot}, equation 18), the total polarizability (α_{tot}, equation 19), the parameters $\Delta\alpha$ (equation 20), and β_0 (equation 21), were done using the exchange-correlation hybrid functional B3LYP, the short-range hybrid functional CAM-B3LYP [54, 55], and the two long-range hybrid functional LC-BLYP [56] and the ωB97XD [57] with methanol as an implicit solvent for each DFT functional. To evaluate the nonlinear optical properties, the urea molecule was used as reference and it was optimized at B3LYP/6–311++G(d,p) in methanol as an implicit solvent and the NLO properties were computed using the same functional as for the amentoflavone.

$$\mu_{tot} = \left(\mu_x^2 + \mu_y^2 + \mu_z^2\right)^{1/2} \tag{18}$$

$$\alpha_{tot} = \frac{1}{3}\left(\alpha_{xx} + \alpha_{yy} + \alpha_{zz}\right) \tag{19}$$

$$\Delta\alpha = \frac{1}{\sqrt{2}}\left[\left(\alpha_{xx} - \alpha_{yy}\right)^2 + \left(\alpha_{yy} - \alpha_{zz}\right)^2 + \left(\alpha_{zz} - \alpha_{xx}\right)^2 + 6\alpha_{xz}^2 + 6\alpha_{xy}^2 + 6\alpha_{yz}^2\right]^{1/2} \tag{20}$$

$$\beta_0 = \left[\left(\beta_{xxx} + \beta_{xyy} + \beta_{xzz}\right)^2 + \left(\beta_{yyy} + \beta_{yzz} + \beta_{yxx}\right)^2 + \left(\beta_{zzz} + \beta_{zxx} + \beta_{zyy}\right)^2\right]^{1/2} \tag{21}$$

2.2. Docking analysis

The docking simulation differs from DFT calculations because this method is based on molecular mechanics. The ligand-receptor molecular recognition process is driven by enthalpy and entropy effects, being determined by Gibbs free energy (ΔG), which is related to the

dissociation constant (K_d), an experimental measure of ligand-receptor interaction (macromolecule) (eq.22).

$$\Delta G = \Delta H - T\Delta S = -RT \ln K_d \quad (22)$$

Where ΔH is the enthalpy variation, T is the absolute temperature, ΔS is the entropy variation and R is the universal gas constant [58]. Therefore, in order to study how the ligand will bond on the target molecule, it is important to define which molecule will be the ligand and the target [59].The AutoDock Vina Code [60] was used to simulate molecular docking between amentoflavone and Cruzain (therapeutic target, enzyme involved in the evolutionary cycle of Trypanosoma cruzi). The crystalline protein structure complexed with inhibitor were obtained from the Protein Data Bank repository (http://www.rcsb.org/pdb/home/home.do) under the codes PDB 3IUT (Cruzain/Tetrafluorophenoxymethyl Ketone (KB2)) [61]. The amentoflavone structure used for docking was optimized by DFT. As a reference molecule, in addition to inhibitors already complexed in the PDB itself, benznidazole (BZN) (ChemSpider ID 29299) was used.

In preparatory step, non-protein molecules were removed from the protein structure, polar hydrogens were added. The grid box parameters for Cruzain: *center_x* = 6.612, *center_y* = -0.436, *center_z* = 8.052, *size_x* = 116, *size_y* = 106, *size_z* = 126, *spacing* = 0.431 e *exhaustiveness* = 8. One hundred independent simulations were carried out using the Lamarckian genetic algorithm. The docking results were clustered into groups with RMSD(Root-mean-square deviation) lower than 2.0 Å [62]. To ensure the docking validity, a redocking procedure was conducted in same Auto Dock Vina [63] software under the same conditions shown before, but now using the native ligands from PDB structure [64]. From the distances obtained, the data were computed and plotted on the web-based tool, Morpheus (https://software.broadinstitute.org/morpheus/), and heat-maps were used to visualize changes in the ligand-residue interaction profiles (L-R's), being evaluated by the Pearson statistical test to detect similarity. The types of chemical interactions L-R's were analysed, and the maps were generated using the Discovery Studio ® software [65]. To render 2D interaction maps, the codes Discovery Studio Visualizer (https://www.3ds.com/) and Ligplot + v.2.2 (https://www.ebi.ac.uk/thornton-srv/software/LigPlus/) were used.

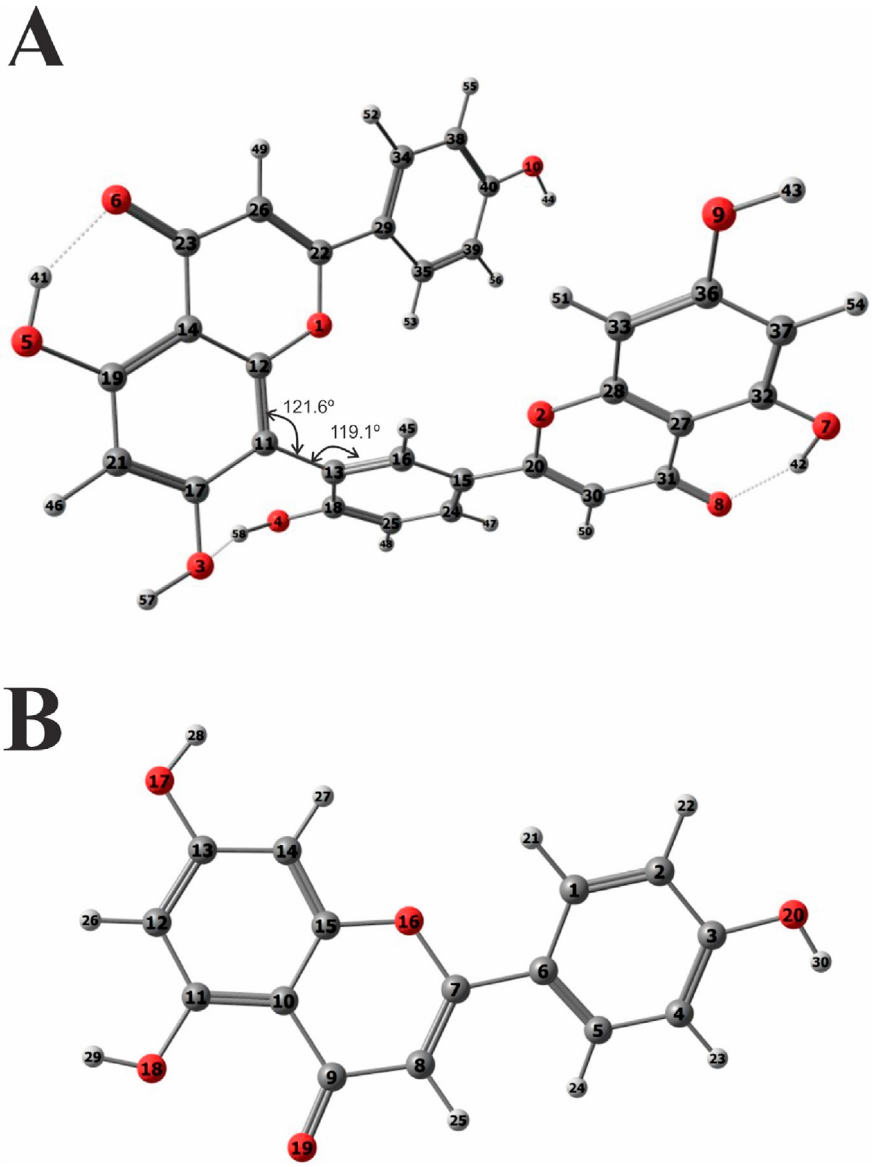

Figure 1. Optimized structures for amentoflavone (A) and apigenin (B) calculated by the DFT method using B3LYP functional and 6–311++G(d,p) basis set.

3. Results and discussion

3.1. DFT results

3.1.1. Geometric structure

Figure 1 shows the optimized structures for amentoflavone (1A) and apigenin (1B) obtained by the DFT method using the B3LYP functional and 6–311++G(d,p) basis set in methanol as an implicit solvent. The sketches of the optimized structures for both molecules were obtained by the trial version of Chemcraft - graphical software for visualization of quantum chemistry computations version 1.8 software (https://www.chemcraftprog.com). The minimum electronic energies for those two molecules are respectively –1196574.269 Kcal.mol^{-1} and – 598656.113 Kcal.mol^{-1} for amentoflavone and apigenin. Two apigenin molecules react to yield one molecule of amentoflavone through the formation of a covalent bond between C14 from one apigenin molecule and C2 from the other apigenin molecule. The structure of the amentoflavone molecule displays a torsion angle of 52.7° between atoms C11–C12–C13–C16. When the two monomer structures are bonded, the dimer structure is not planar, as seen in Figure 1, and there is a cavity between the two monomers with the angles C11–C12–C13 of 121.6° and C11–C13–C16 of 119.1°. Thus, the structure is stable in this configuration due to the intramolecular hydrogen bond between O3–H58 (d = 1.92724 Å), O6–H41 (d = 1.66738 Å), and O8–H42 (d = 1.68654 Å). This cavity has an important biological implication, either through interaction with an amino acid residue or interactions with solvent molecules that further stabilize the dimer. To comprehend the importance of the cavity in the amentoflavone molecule, the optimization was done additionally using diverse implicit solvents with different values of dielectric constant as seen in Table S1 (supplementary material). It can be observed that regardless of the value of the polarity of the solvent, the torsion angle and the dihedral angles of amentoflavone molecule remains approximately constant. This occurs due to the intramolecular hydrogen bond between O3–H58 atoms that stabilizes the structure in this conformation with an average torsion angle around 52.72° for C11–C12–C13–C16 and average dihedrals angles around 119.068° for C11–C13–C16 and 121.557° for C11–C12–C13. The distance between the oxygen atom O3 and the hydrogen atom H58 changes slightly with the polarity of the solvent ($d_{average}$ = 1.92791 Å), however, this change is small to break the hydrogen bond. Thus, these data suggest that the amentoflavone molecule keeps this cavity in different chemical environments. The phenyl group can spin around the bond C29–C22, and the benzopyranone group can spin around the bond C20–C15. These groups can fit their position depending on the type of molecule within the cavity to achieve an extra stabilization. Pan *et al.* [11] studied the optimization of amentoflavone molecule in the gas phase, and they reported that the torsion angle between the two monomer structures was about -114.4° and this conformation probably does not allow the formation of the third hydrogen bond. In this work, this hydrogen bond is represented by the bond between O3 and H58 atoms which occurs due to the angulation between the monomeric structures.

3.1.2. Infrared and thermodynamic analysis

It is known from the experimental studies that infrared spectroscopy is one of the efficient methods to characterize the molecular structure. In this work, the infrared spectrum was used to assess whether the calculated geometry for the amentoflavone is located at the true minima of potential energy. The experimental wavenumbers from amentoflavone infrared spectrum were obtained from the work of Yeh *et al.* [66] and they were correlated with the calculated wavenumbers in methanol as an implicit solvent as seen in Table S2 (supplementary material). As a result of the electron correlation and basis set deficiencies [67], the theoretical wavenumbers are frequently higher than the experimental corresponding values. To reduce the discrepancy from theoretical value to the experimental ones, an appropriated scaling factor is introduced by measuring the anharmonic corrections explicitly. The theoretical wavenumbers were scaled by 0.967 at the B3LYP/6–311++G(d,p) level of theory and the assignments were done using the using the VEDA 4 software [30] to compute the Potential Distribution Energy (PED), and it was only considered PED $\geq$ 10% for the theoretical assignment. Considering the vibrational mode with the higher PED for each wavenumber, the band at 847.305 cm^{-1} is the torsion of the H41–O5–C19–C14 out of the molecular plane; the band at 1070.39 cm^{-1} are the bending in plane of C25–C24–C15 and C15–C16C-13; the band at 1126.457 cm^{-1} is the bending in molecular plane of H49–C26–C23; the band at 1224.273 cm^{-1} are the bending in plane of H58–O4–C18 and the stretching of the C18–C25; the band at 1289.705 cm^{-1} is the stretching of O10–C40 between the phenyl ring and the hydroxyl group; the band at 1517.363 cm^{-1} are the bending in plane of the H46–C21–C19 and the H41–O5–C19; the band at 1534.232 cm^{-1} is the in plane bending of H52–C34–C38, H55–C38–C40, H56–C39–C30, H53–C35–C39; the band at 1621.47 cm^{-1} is the stretching of the C29–C35 and C39–C40; the band at 1668.765 cm^{-1} are stretching of the C12–C14 and C19–C21 and the in plane bending of the H41–O5–C19; the band at 1674.313 cm^{-1} are the in plane bending of the C27–C28–O2; the bands at 3160.247 cm^{-1}, 3194.128 cm^{-1}, and 3691.628 cm^{-1} are related to the hydroxyl group stretching O5–H41, O7–H42 and O4–H58 respectively. From the results seen bellow, the calculated wavenumbers are in satisfactory agreement with the experimental wavenumbers, being possible to obtain a mathematical linear correlation (Eq. 23) which presented a correlation coefficient (R^2) of 0.9994 (Figure 2) and it demonstrates that the theoretical optimized structure of amentoflavone describes its real molecular structure.

$$y = 1.0563x - 77.957 \tag{23}$$

The thermodynamic properties are significant in the studies of chemical species since they are related to the formation of the compound itself. It is widely known that Gibbs's free energy is used to determine thermodynamic stability, since it takes in account the enthalpic and entropic factors. Thus, as can be observed in Table 1, the value Gibbs free energy for the reaction of dimerization for the amentoflavone assume a negative value, which implies that the dimerization of apigenin to yield amentoflavone molecule is thermodynamically favourable.

3.1.3. Frontier Molecular Orbitals and reactivity descriptors analysis

The reactivity descriptors calculated for the amentoflavone and apigenin molecules are shown in Table 2. The apigenin's HOMO orbital has energy value ($E_{HOMO} = -6.3463\ eV$) slightly lower than the amentoflavone's HOMO energy value ($E_{HOMO} = -6.2932\ eV$), suggesting that the valence electron density distribution for amentoflavone is more available to be donated then apigenin molecule, hence the amentoflavone should be more reactive. Nonetheless, the amentoflavone's LUMO orbital has energy value ($E_{LUMO} = -2.3315\ eV$) lower than the apigenin's LUMO orbital ($E_{LUMO} = -2.0612\ eV$), which means that amentoflavone is more susceptible to accept electronic density since the additional electron will be described by a lower energy molecular orbital. Therefore, the amentoflavone molecule should be more reactive than apigenin. This tendency can be observed using the HOMO-LUMO energy gap (ΔE_{Gap}) since the reactivity of a chemical species is related directly to the lower energy difference (lower energy gap). The amentoflavone's energy gap ($\Delta E_{Gap} = 3.9617\ eV$) is lower than the apigenin's energy gap ($\Delta E_{Gap} = 4.2851\ eV$), which implies more chemical reactivity to the amentoflavone as seen in Figure 3 the isosurfaces of the HOMO and the LUMO and the energy difference. In this perspective, due to the higher energy value of the HOMO, the amentoflavone holds its electronic density weaker than apigenin, which corresponds to lower ionization energy as seen in Table 2. Amentoflavone molecule has a higher electron affinity (A = 2.3315 eV) than apigenin (A = 2.0612 eV) due to the lower energy value of the LUMO as it was described above. Both molecules demonstrated chemical stability due to the negative value of chemical potential.

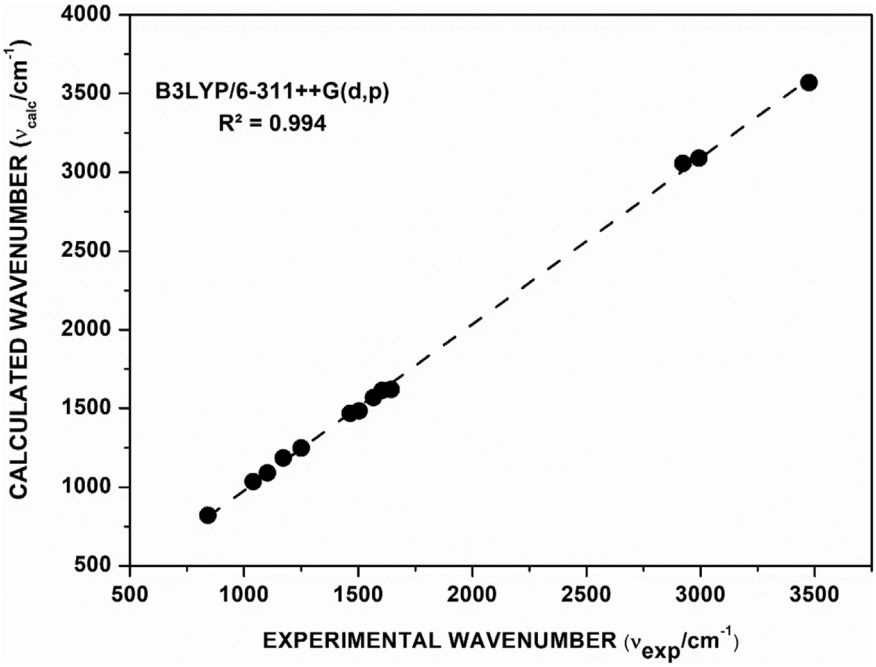

Figure 2. Liner correlation between the calculated and experimental wavenumber for the infrared spectrum of amentoflavone.

Table 1. Calculated Thermodynamic properties of Amentoflavone and Apigenin by B3LYP/6–311++G(d,p) level of theory.

	Internal Energy (U/Kcal.mol^{-1})	Enthalpy (H/Kcal.mol^{-1})	Entropy (S/Kcal.mol^{-1})	Gibbs Free Energy (G/Kcal.mol^{-1})
Amentoflavone	283.602	831.406	0.206	770.065
Apigenin	147.884	434.111	0.130	395.411

Table 2. Calculated reactivity descriptors values of Amentoflavone and Apigenin by B3LYP/6–311++G(d,p) method.

Quantum reactivity descriptor	Amentoflavone	Apigenin
E_{HOMO} (eV)	-6.2932	-6.34633
E_{LUMO} (eV)	-2.3315	-2.06122
n E_{Gap} (eV)	3.9617	4.2851
I (eV)	6.2932	6.3463
A (eV)	2.3315	2.0612
χ (eV)	4.3124	4.2038
μ (eV)	-4.3124	-4.2038
η (eV)	1.9809	2.1426
S (eV^{-1})	0.5048	0.4667
ω (eV)	4.6940	4.1240
ε (eV^{-1})	0.2130	0.2425

According to the Pearson's HSAB theory [68,69] a favourable interaction between two compounds occurs when both are hard or soft molecules [70], thus apigenin molecule is considered hard due to the value of global hardness (η = 2.1426 eV) or low value of global softness (S = 0.4667 eV^{-1}) and the reaction between them, in consequence, the formation of amentoflavone, is favourable. Both reactivity descriptors electronegativity and electrophilicity index for amentoflavone ($\chi = 4.3124\ eV$ and $\omega = 4.6940\ eV$) has higher values than those calculated for apigenin ($\chi = 4.2038\ eV$ and $\omega = 4.1240\ eV$). Therefore, the amentoflavone molecule is more susceptible to accept electronic density, which can be classified as a good electrophilic species, in comparison to apigenin molecule, which has higher value of nucleophilicity index ($\varepsilon = 0.2425\ eV^{-1}$).

To understand the effect of the chemical environment on the reactivity of amentoflavone, the energy gap for each solvent, which this molecule was optimized, was obtained using the energy values of the HOMO and LUMO, thus the results are shown in Table 3. When the polarity of the solvent increases, the total electronic energy of amentoflavone molecule decreases slightly. The energy gap changes slightly with the increase of the polarity of the solvent, thus, the amentoflavone molecule is more reactive in non-polar solvents and it is slightly more stable in polar solvents. Therefore, this table provides relevant information for choosing appropriate solvents to perform pharmacokinetic and pharmacodynamic studies.

3.1.4. *Fukui functions and local molecular descriptors analysis*

The results of the condensed Fukui functions, the dual and the multiphilic descriptors are shown in Table S3 at the supplementary material. The electronic Fukui functions for nucleophilic attack (f^+), for electro-

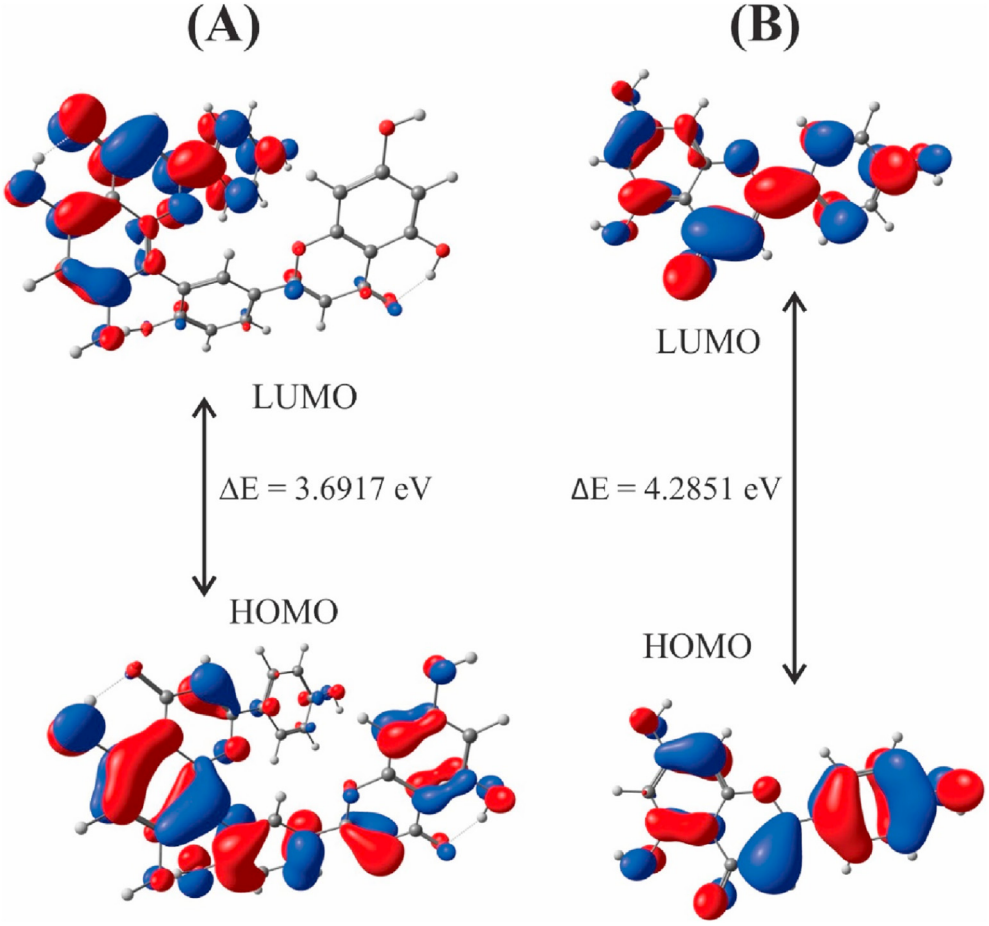

Figure 3. Drawn illustrating the distribution map of the frontier orbitals and the gap energies (ΔE_{Gap}) of Amentoflavone (A) and Apigenin(B).

Table 3. HOMO energy value, LUMO energy value, energy gap (n E_{gap}) and total electronic energy (Eh) for amentoflavone calculated taking in account the dielectric constant of several solvents by B3LYP/6–311++G(d,p) level of theory.

Solvent	HOMO (eV)	LUMO (eV)	Energy Gap (n E_{gap})	Total Electronic Energy (Eh)
Water	-6.2930	-2.3315	3.9615	-1906.8649
DMSO	-6.2932	-2.3315	3.9617	-1906.8644
DMF	-6.2932	-2.3315	3.9617	-1906.8641
Acetonitrile	-6.2932	-2.3315	3.9617	-1906.8641
Methanol	-6.2932	-2.3315	3.9617	-1906.8639
Ethanol	-6.2935	-2.3318	3.9617	-1906.8634
Acetone	-6.2938	-2.3318	3.9620	-1906.8629
Pyridine	-6.2946	-2.3320	3.9626	-1906.8615
CH_2Cl_2	-6.2954	-2.3329	3.9626	-1906.8598
THF	-6.2957	-2.3337	3.9620	-1906.8587
Chloroform	-6.2973	-2.3369	3.9604	-1906.8552
Toluene	-6.3014	-2.3522	3.9492	-1906.8475
CCl_4	-6.3017	-2.3549	3.9468	-1906.8466
Hexane	-6.3033	-2.3631	3.9402	-1906.8441

philic attack (f^-) and the isosurface of the dual descriptor (n f) were plotted using the VESTA 3 software [52], they are shown in Figure 4a, b and Figure 5 respectively. The yellow and the blue isosurfaces corresponds to the negative and positive signs of condensed function and dual descriptor function, respectively. It is possible do conclude that the following atoms O3, O4, O5, O7, O9, C11, C12, C13, C14, C15, C16, C17, C18, C19, C21, C24, C25, C27, C28, C30, C32, C33, C36 and C37 are electrophilic sites, in other words, it is prone to nucleophilic attack because they have both Δf and Δω > 0. Whereas, O1, O2, O6, O8, O10, C20, C22, C23, C26, C29, C31, C34, C35, C38, C39 and C40 are nucleophilic sites, this means that it is prone to electrophilic attack because they have both Δf and Δω < 0. The atoms C22, C23 and O6 have the higher value of dual and multiphilic descriptors (in modulus) and they are the most susceptible to electrophilic attack, although the atom C33 has the higher value of Δf and Δω and it is the most susceptible to nucleophilic attack. The electronic Fukui functions (Figures 4a and b) confirm the results predicted by the condensed Fukui functions computed from the Hirshfeld atomic charge population.

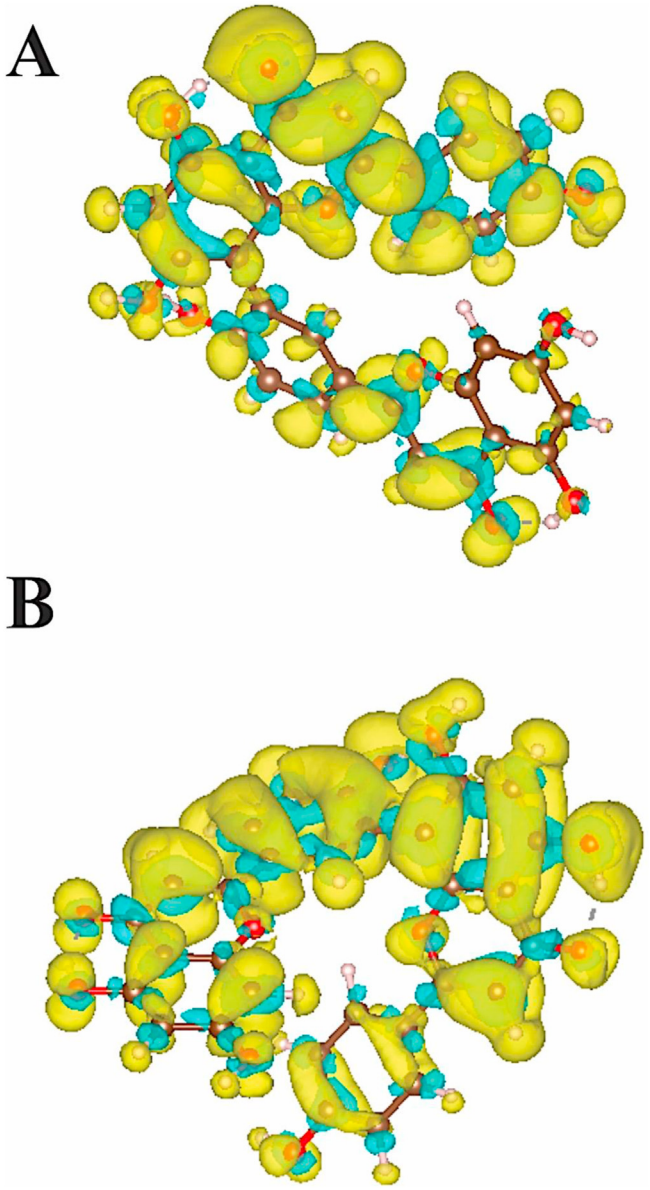

Figure 4. Illustrative drawing showing the isosurfaces of amentoflavone. Yellow and blue colours correspond to negative and positive signs of condensed function of amentoflavone for nucleophilic attack (f^+) (A) and electrophilic attack (f^-) (B), respectively.

3.1.5. Nonlinear optical properties

To expand the study of the applications of the amentoflavone molecule beyond the biological use, the nonlinear optical (NLO) calculations for the amentoflavone molecule were done using the DFT methods B3LYP, CAM-B3LYP, LC-BLYP, and ωB97CD with the 6–311++G(d,p) basis set using methanol as an implicit solvent and the results are shown in Tables S5 – S8. The reference molecule (urea) was optimized and the NLO properties were computed at the same level of theory as for the amentoflavone. The values for the parameters as follow total polarizability (α_{tot}), Δα, and β_0 when compared between the amentoflavone and the urea molecule assume values respectively 14.716, 21.737, and 111.675 times greater than urea for the B3LYP; 14.325, 20.789, and 153.579 greater than urea for the CAM-B3LYP; 14.099, 19.934, and 146.596 times greater than urea for the LC-BLYP; 14.333, 20.696, and 129.592 times greater than urea for the ωB97XD. These results show that the amentoflavone molecule can be used in optoelectronic devices since its nonlinear optical properties are greater than the reference molecule.

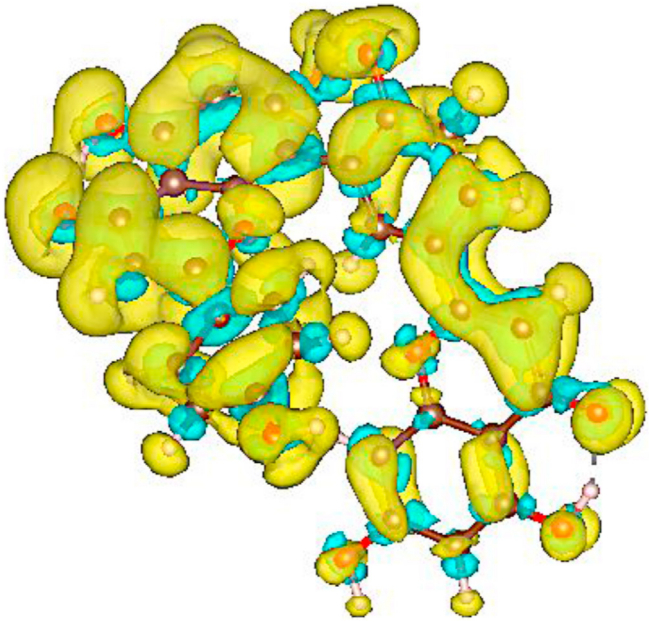

Figure 5. Illustrative drawing showing the isosurfaces of amentoflavone. Yellow and blue colours correspond to negative and positive signs of condensed Fukui function of amentoflavone for dual descriptor (Δf), respectively.

The four DFT methods were also compared and the results are shown in Table S9. All the DFT methods are very similar to predict the NLO properties, hence all four methods used can be satisfactory use to describe the optical behaviour of the amentoflavone molecule.

3.2. Docking results

The routines validation criterion of the docking was Room Means Square Deviation (RMSD), with ideal values below 2.0 Å[62], which showed that amentoflavone presented values ideal in all simulations (RMSD: Cruzain = 0.990 Å). Also, as a validation criterion, affinity energy values were used, with reference values lower than -6.0 kcal/mol [71]. Amentoflavone also showed optimal results in all affinity simulations (-8.0 kcal/mol), given that the lower the affinity value of the binder conformation in the molecular coupling, the more favorable is the bond found [72]. Cruzain, the main cysteine protease enzyme of *T. cruzi*, essential for intracellular parasite replication, is considered one of the most important targets for the search for new trypanocidal agents [72]. The molecular docking results of amentoflavone and Cruzain, as well as comparative couplings with BZN and Tetrafluorophenoxymethyl Ketone Inhibitor (KB2) complexed with the cruzain enzyme, show amentoflavone in the region near the binding site of KB2 (Figure 6), inferring a potential inhibitory effect of cruzain. Cruzain has a catalytic site located at the intersection of two domains, one predominantly composed of α-helices and the other of antiparallel β-Sheets, where the residues stand out (Glu208, Gly66, Asp161, Gln19, His162, Cys25) (Figure 7), with distances of 4.7 Å, 4.5 Å, 4.2 Å, 3.8 Å, 3.8 Å and 4.0 Å, respectively (Table S4 supplementary material). It was also highlighted Trp184 residue that play an important role in inhibitor binding [61,72].

In order to better demonstrate the results obtained in this work, a heat map was constructed with the data on distance and forces of interaction between ligands and receptors (Figure 8). Heatmaps of the different interaction forces between all ligands and their respective reactive amino acids, legitimizing three (3) important regions of interaction at the active site of KB2, protein 3IUT, characterizing strong and weak links between them. Hierarchical groupings demonstrated in Figure 8A, from the shortest distances (red) of interaction to the greatest distances (blue). Shaded in orange are the residues that play an important role in the

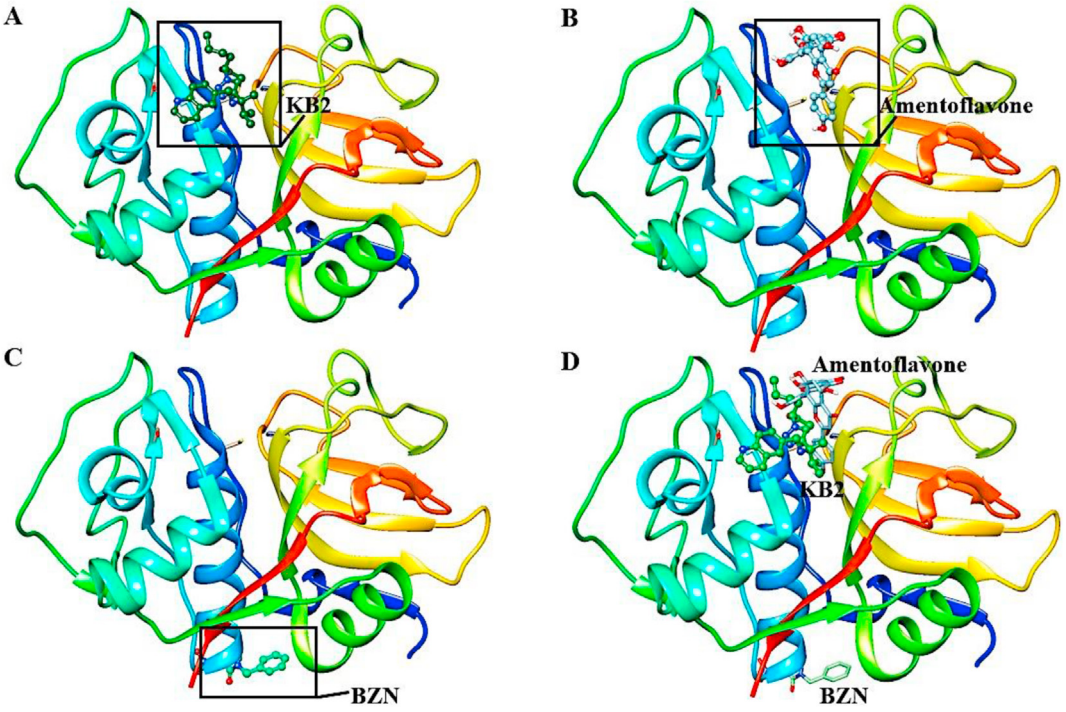

Figure 6. Schematic 2-D representations the Cruzain complexes with Tetrafluorophenoxymethyl Ketone Inhibitor (KB2) (A), Docking between Cruzain and Amentoflavone (B), between Cruzain and Benznidazole (BZN) (C) and binding site of Amentoflavone, BZN and KB2 in the Cruzain (D).

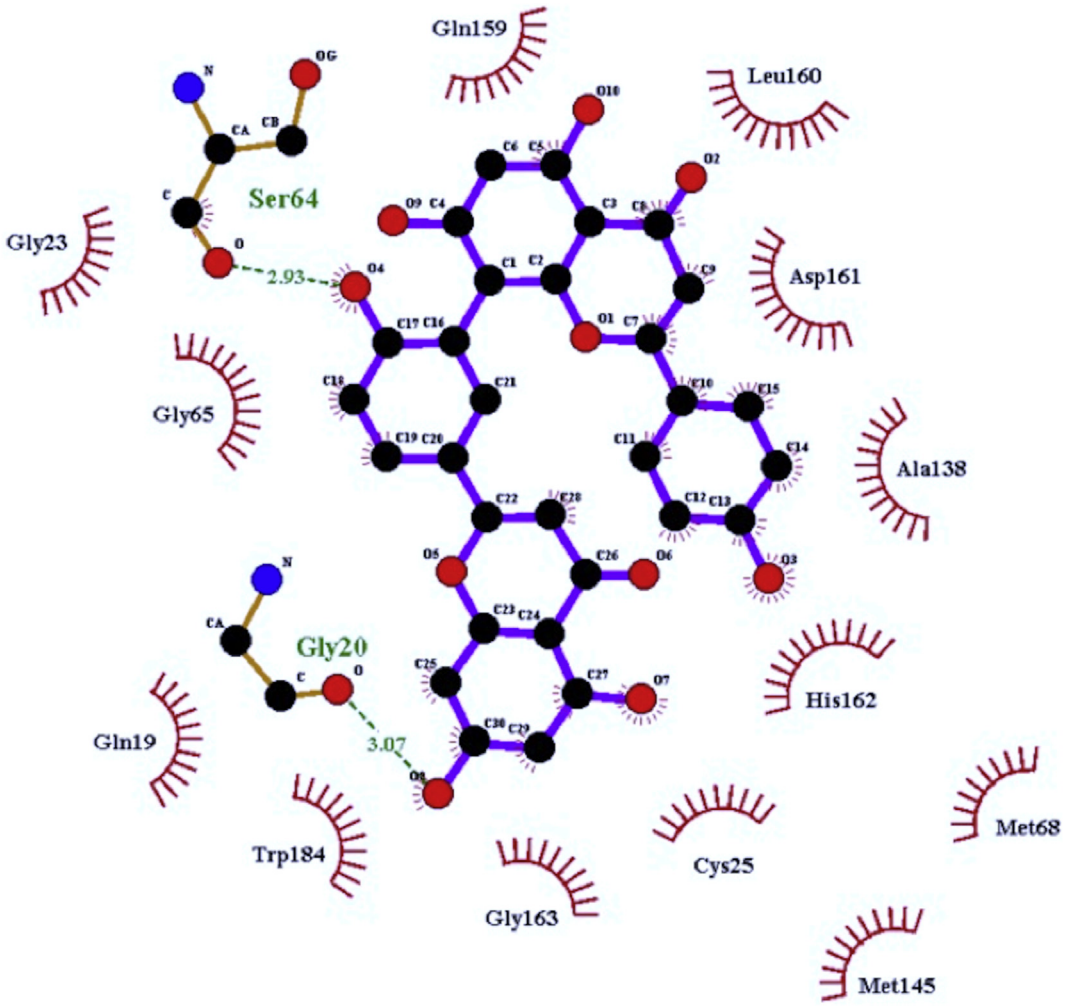

Figure 7. Schematic 2-D representations of cruzain-amentoflavone complex.

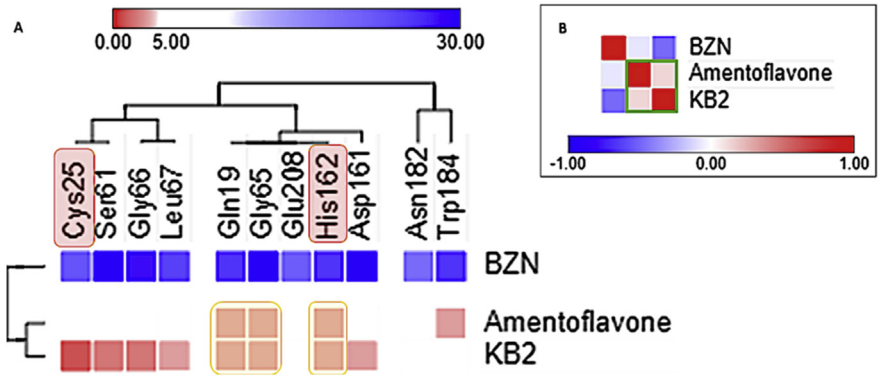

Figure 8. Schematic representations of heatmaps of the different interactions expressed between the binders and the crosshair. (A) Important regions of interaction at the active site of KB2 and protein 3IUT. (B) Similarity test between the Amentoflavone and KB2 ligands, where, BZT is isolated. Values identified between blue and white in the Pearson similarity test correspond to the significance value $P < 0.05$.

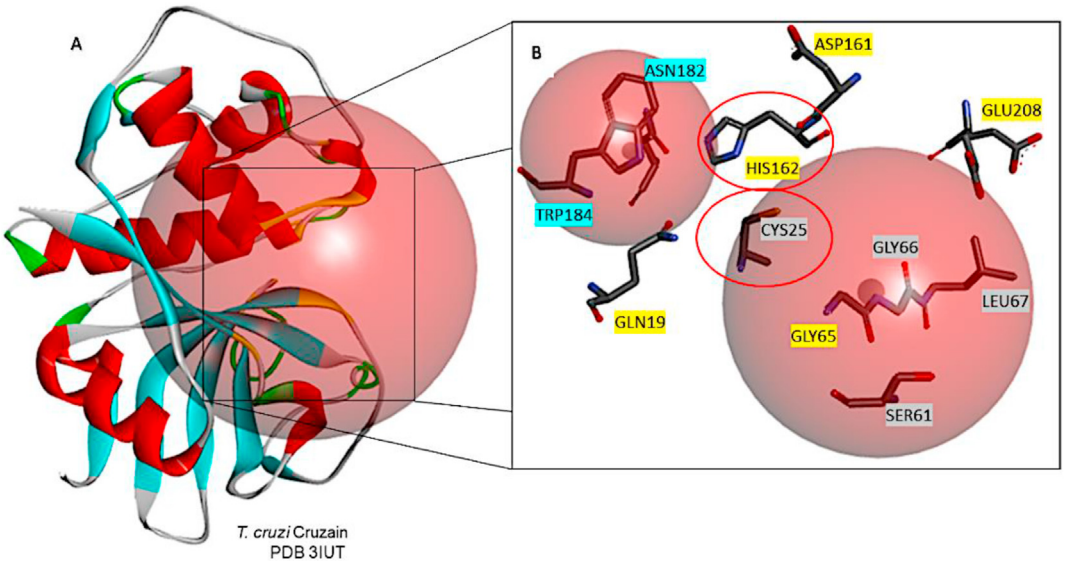

Figure 9. Schematic 2-D representations showing the crosswalk extracted from protein data bank structure in ribbon format (cruzain (PDB 3IUT)), active site KB2 shown by red circle and activity residues in yellow (A). Amino acids from the KB2 site in evidence. Circled in red are the residues that play an important role in the ligand-receptor connection at the KB2 site (B).

ligand-receptor connection at the KB2 site. In yellow, residues that showed similar relationships between different ligands.

Figure 8B heatmap provides Pearson's similarity test between the Amentoflavone and KB2 ligands, where, BZT is isolated. In the layout, the closer to 1 (red) the interaction force will be more determinant and intense, the closer to -1 (blue) the greater the distance and the interaction force will be negligible. Grouping highlighted by green square. When analysing the referred heat map, it was also possible to perceive that the following groups were formed: 3 clusters between the amino acids (X-axis) and 2 clusters between the substances (Y-axis). The amentoflavone ligand approaches the KB2 reaction site, not interacting with the BZN binding site and confirming the site proposed by Pavão and collaborators [61]. In addition, on the nucleophiles responsible for the connection between ligand and receptor (LR), regardless of the interaction forces, amentoflavone interacted with all the amino acids of the KB2 site, unlike BZN, making it possible to identify a possible synergistic activity during treatment. with amentoflavone and BZN. Yet, despite the fact that Cys25 and His162 residues are considered essential in the chemical coupling of therapeutic substances [61], in this study, the importance of Gln19 and Gly65 residues was also evident, even though the interactions occurred between them and the ligands considered to be of low or moderate intensity (Figure 8A). When it was evaluated the ligands with each other using Pearson's similarity test (Figure 8B) it was once again able to corroborate the identification of the amentoflavone ligands proximity to KB2, shown in green, to the detriment of BZN.

Figure 9 (A) shows the complete structure of Cruzain with a yellow highlighted link to Figure 9 (B), where the interaction residues were evidenced showing the presence of three nuclei (gray, yellow and blue) of distinct activity in the same catalytic site. The residues identified by gray or blue are further apart while the ligands KB2 and amentoflavone fit on the left in residues Cys25 and His 162, these residues being the most important for KB2. This ligand shares similarity of importance with the residues Gln19, Gly 65, His162 which, for amentoflavone, function as a catalytic triad in the protein cavity to which the two ligands attach. It can also be seen that each of the fundamental residues for KB2 is arranged in a specific group constructed from the statistical information found in Figure 8 (A) and with that data, Figure 10. Where in the layout, the closer to 1 (white) the interaction force will be more determinant and intense, the closer to -1 (black) the greater the distance and the interaction force will be negligible. Groupings highlighted by red squares

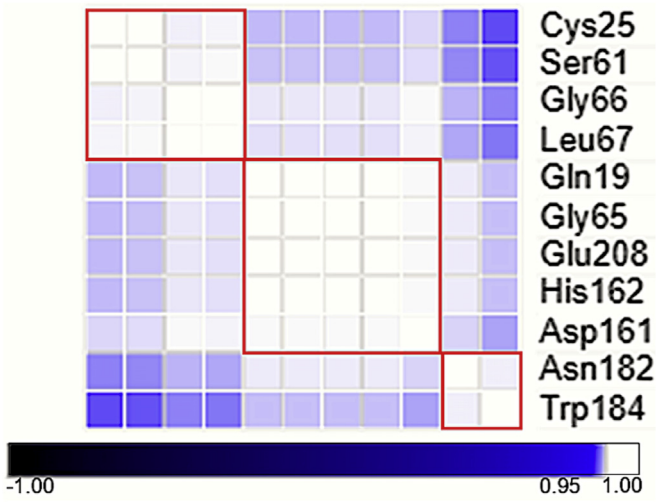

Figure 10. Heatmap demonstrating Pearson's similarity test between reactive amino acids in the cruzain-amentoflavone complex. Values identified between blue and white in the Pearson similarity test correspond to the significance value $P < 0.05$.

corroborate the results obtained in Figure 10. Nonspecific residues highlighted by squares shaded in yellow. In this image it can be see clearly the evidence of the formation of the three main characteristic groups for this target and evaluated ligands.

Based on the simulation that presented the shortest distance between the ligand and the catalytic site, it was possible to identify and evaluate the interactions between amentoflavone and cruzain, being possible to identify a π-π Stacked interaction with the residue TRP184 (3.4 Å), an interaction of van der Waals with HIS162 (3.8 Å), a Pi-Alkyl with ALA138 (3.77 Å), an Amide-Pi Stacked with the ASP161 residue (4.2 Å) and three hydrogen bonds with the GLY20 (3.07 Å), SER64 (2.93 Å) and MET68 (3.05 Å), which are classified as strong according to the distances, indicating an important route of inhibition (Figure 11).

4. Conclusion

The structural geometrical optimization using several solvents with different values of dielectric constant was made to amentoflavone molecule and it was found that regardless of the value of the polarity of the solvent, the torsion angle and the dihedral angles of amentoflavone molecule varies slightly. The excellent linear correlation, between the experimental and calculated infrared wavenumbers, shows that the theoretical optimized structure of amentoflavone describes the actual molecular structure. The energy gap changes slightly with the increase of the polarity of the solvent, thus, the amentoflavone molecule is more reactive in non-polar solvents and it is slightly more stable in polar solvents. By using Fukui charge analysis (the condensed Fukui functions) it was possible to identify the nucleophilic and electrophilic regions. Additionally, the amentoflavone molecule exhibits excellent nonlinear

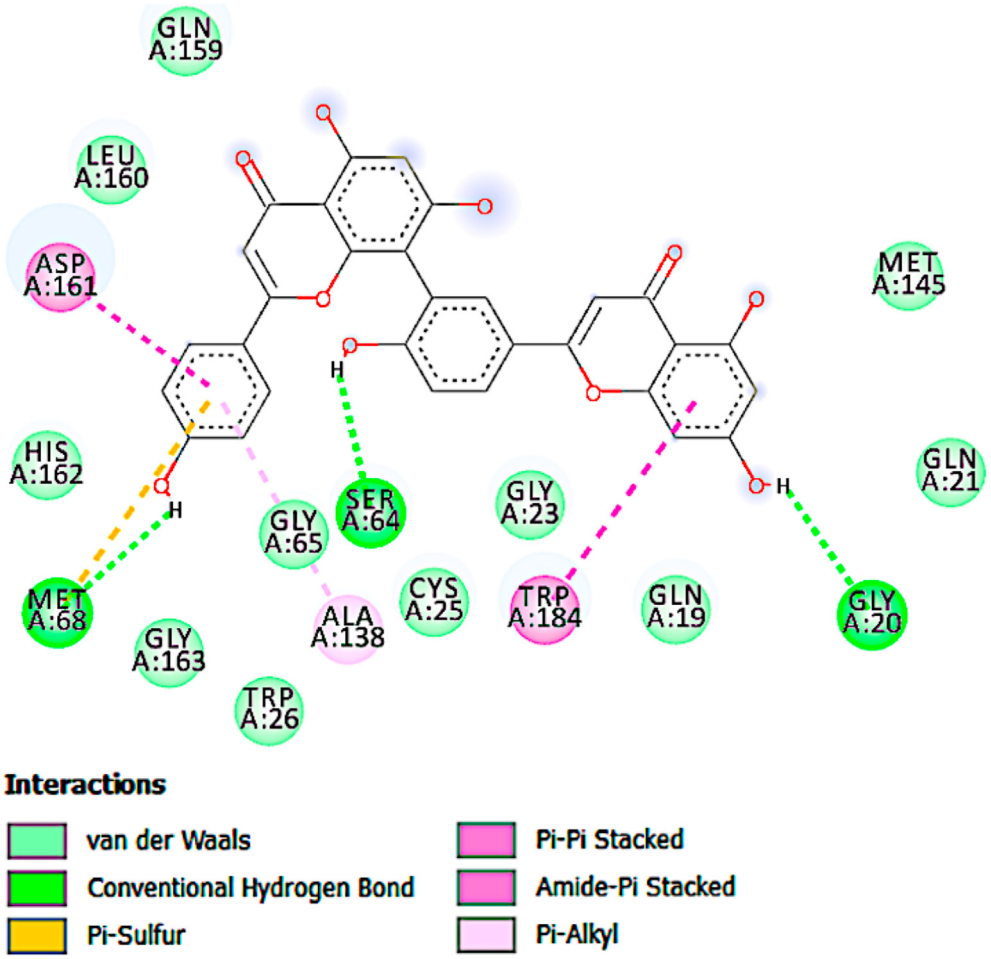

Figure 11. 2D map representative of the main interactions between amentoflavone and Cruzain amino acid residues.

optical response, hence this molecule can be used in optical devices. The molecular docking result demonstrated, the interaction of amentoflavone with amino acid residues present in the catalytic site of enzyme, that is, it interacted in the region near the site occupied by inhibitors already complexed with Cruzain. This result suggests that amentoflavone has the potential to interfere with the enzymatic activity of cruzain, thus being an indication of being a promising antichagasic agent. Therefore, these data are essential to understand the biological application of this compound and in the development of protocols for pharmacokinetic and pharmacodynamic tests, as well as in the development of new drugs (drug design).

Declarations

Author contribution statement

Ricardo Santos, Alice Martins: Conceived and designed the experiments; Wrote the paper.

Emmanuel Marinho, Pedro de Lima Neto: Conceived and designed the experiments; Analyzed and interpreted the data; Wrote the paper.

Márcia Marinho, Francisco Wagner: Performed the experiments; Analyzed and interpreted the data; Wrote the paper.

Leonardo Silva: Performed the experiments; Analyzed and interpreted the data.

Ramon Menezes: Analyzed and interpreted the data; Wrote the paper.

Funding statement

This work was supported by Coordenação de Aperfeiçoamento de Pessoal de Nível Superior. Márcia Machado Marinho was supported by Conselho Nacional de Desenvolvimento Científico e Tecnológico.

Data availability statement

Data included in article/supplementary material/referenced in article.

Declaration of interests statement

The authors declare no conflict of interest.

Additional information

Supplementary content related to this article has been published online at https://doi.org/10.1016/j.heliyon.2021.e06079.

Acknowledgements

The authors also thanks Centro Nacional de Processamento de Alto Desempenho (CENAPAD) of the Federal University of Ceará (UFC) for providing computational resources.

References

[1] 3. López-Vélez, Francesca F. Rogelio, Norman, Cb, American Trypanosomiasis 2020, 2020.
[2] E. Chatelain, J.R. Ioset, Drug discovery and development for neglected diseases: the DNDi model, Drug Des. Dev. Ther. 5 (2011) 175.
[3] G. Murillo-Godínez, Chagas disease (American trypanosomiasis), Med. Int. Mex. 34 (6) (2018) 959–970.
[4] E. Chatelain, Chagas disease drug discovery: toward a new era, J. Biomol. Screen 20 (1) (2015) 22–35.
[5] E.F. da Silva-Junior, P.H. Barcellos Franca, F.F. Ribeiro, et al., Molecular docking studies applied to a dataset of cruzain inhibitors, Curr. Comput. Aided Drug Des. (2017) 68–78.
[6] E.I. Erreira, Drug design for chagas'disease: advances and challenges, Rev Virtual Quim 4 (3) (2012) 225–246.
[7] M.M. Marinho, R. Pires, D.O.S. Santos, et al., Molecular fractionation with conjugate caps study of the interaction of the anacardic acid with the active site of trypanosoma cruzi gapdh Enzyme : a quantum investigation, Asian J. Pharmaceut. Clin. Res. 12 (12) (2019).
[8] W. De Azevedo Jr., MolDock applied to structure-based virtual screening, Curr. Drug Targets 11 (3) (2010) 327–334.
[9] L.H. Madkour, S. Kaya, L. Guo, C. Kaya, Quantum chemical calculations, molecular dynamic (MD) simulations and experimental studies of using some azo dyes as corrosion inhibitors for iron. Part 2: bis–azo dye derivatives, J. Mol. Struct. (2018) 397–417.
[10] E.J. Braga, B.T. Corpe, M.M. Marinho, E.S. Marinho, Molecular electrostatic potential surface, HOMO–LUMO, and computational analysis of synthetic drug Rilpivirine, Int. J. Sci. Eng. Res. 7 (7) (2016) 315–319.
[11] X. Pan, N. Tan, G. Zeng, Y. Zhang, R. Jia, Amentoflavone and its derivatives as novel natural inhibitors of human Cathepsin B, Bioorg. Med. Chem. (2005) 5819–5825.
[12] N. Brooijmans, I.D. Kuntz, Molecular recognition and docking algorithms, Annu. Rev. Biophys. Biomol. Struct. (2003) 335–373.
[13] L.G. Ferreira, R.N. Dos Santos, G. Oliva, A.D. Andricopulo, Molecular docking and structure-based drug design strategies, Molecules (2015) 13384–13421.
[14] D. Selvaraj, S. Muthu, S. Kotha, R.S. Siddamsetty, S. Andavar, S. Jayaraman, Syringaresinol as a novel androgen receptor antagonist against wild and mutant androgen receptors for the treatment of castration-resistant prostate cancer: molecular docking, in-vitro and molecular dynamics study, J. Biomol. Struct. Dyn. (2020) 1–4.
[15] P.M. Cheuka, G. Mayoka, P. Mutai, K. Chibale, The role of natural products in drug discovery and development against neglected tropical diseases, Molecules 22 (1) (2017) 58.
[16] BRAINER MS de CP, VIDAL M de F, Cajucultura nordestina em recuperação, Cad Setorial ETENE 54 (3) (2018) 1–13.
[17] B. Weniger, C. Vonthron-Sénécheau, M. Kaiser, R. Brun, R. Anton, Comparative antiplasmodial, leishmanicidal and antitrypanosomal activities of several biflavonoids, Phytomedicine (2006) 176–180.
[18] J.E. Mbosso Teinkela, X. Siwe Noundou, E.L. Nguemfo, et al., Biological activities of plant extracts from Ficus elastica and Selaginella vogelli: an antimalarial, antitrypanosomal and cytotoxity evaluation, Saudi J. Biol. Sci. 25 (1) (2018) 117–122.
[19] Y.S. Rizk, A. Fischer, Cunha M de C, et al., In vitro activity of the hydroethanolic extract and biflavonoids isolated from Selaginella sellowii on Leishmania (Leishmania) amazonensis, Mem. Inst. Oswaldo Cruz (2014) 1050–1060.
[20] J.J. Hyun, S.S. Woo, S.H. Yeo, et al., Antifungal effect of amentoflavone derived from Selaginella tamariscina, Arch Pharm. Res. (Seoul) 29 (9) (2006) 746–751.
[21] H.J. Jung, K. Park, I.S. Lee, et al., S-Phase accumulation of Candida albicans by anticandidal effect of amentoflavone isolated from Selaginella tamariscina, Biol. Pharm. Bull. 30 (10) (2007) 1969–1971.
[22] K.M. Sakthivel, C. Guruvayoorappan, Amentoflavone inhibits iNOS, COX-2 expression and modulates cytokine profile, NF-κB signal transduction pathways in rats with ulcerative colitis, Int. Immunopharm. (2013) 907–916.
[23] M.J. Frisch, G.W. Trucks, H.B. Schlegel, G.E. Scuseria, M.A. Robb, J.R. Cheeseman, G. Scalmani, V. Barone, G.A. Petersson, H. Nakatsuji, X. Li, M. Caricato, A. Marenich, J. Bloino, B.G. Janesko, R. Gomperts, B. Mennucci, H.P. Hratchian, J.V. Ortiz, A.F. Izmaylov, J.L. Sonnenberg, D. Williams-Young, F. Ding, F. Lipparini, F. Egidi, J. Goings, B. Peng, A. Petrone, T. Henderson, D. Ranasinghe, V.G. Zakrzewski, J. Gao, N. Rega, G. Zheng, W. Liang, M. Hada, M. Ehara, K. Toyota, R. Fukuda, J. Hasegawa, M. Ishida, T. Nakajima, Y. Honda, O. Kitao, H. Nakai, T. Vreven, K. Throssell, J.A. Montgomery, J.E. Peralta, F. Ogliaro, M. Bearpark, J.J. Heyd, E. Brothers, K.N. Kudin, V.N. Staroverov, T. Keith, R. Kobayashi, J. Normand, K. Raghavachari, A. Rendell, J.C. Burant, S.S. Iyengar, J. Tomasi, M. Cossi, J.M. Millam, M. Klene, C. Adamo, R. Cammi, J.W. Ochterski, R.L. Martin, K. Morokuma, O. Farkas, J.B. Foresman, D.J. Fox, Gaussian 09, Revision A.02, 2009.
[24] R. Dennington, T. Keith, J. Millam, GaussView, Version 5, 2009.
[25] A.D. Becke, A new mixing of Hartree-Fock and local density-functional theories, J. Chem. Phys. (1993) 1372–1377.
[26] C. Lee, W. Yang, R.G. Parr, Development of the Colle-Salvetti correlation-energy formula into a functional of the electron density, Phys. Rev. B 37 (2) (1988) 785–789.
[27] A.D. Becke, A real-space model of nondynamical correlation, J. Chem. Phys. 122 (2003), 064101.
[28] R. Ditchfield, W.J. Hehre, J.A. Pople, Self-consistent molecular-orbital methods. IX. An extended Gaussian-type basis for molecular-orbital studies of organic molecules, J. Chem. Phys. 54 (2) (1971) 724.
[29] E. Cancès, B. Mennucci, J. Tomasi, A new integral equation formalism for the polarizable continuum model: theoretical background and applications to Isotropic and anisotropic dielectrics, J. Chem. Phys. 107 (1997) 3032–3041.
[30] H. Jamroz Michal, Vibrational Energy Distribution Analysis VEDA 4, 2010.
[31] S. Grimme, Supramolecular binding thermodynamics by dispersion-corrected density functional theory, Chem. Eur J. 18 (32) (2012) 9955–9964.
[32] S. Suresh Kumar, S. Athimoolam, B. Sridhar, XRD, vibrational spectra and quantum chemical studies of an anticancer drug: 6-Mercaptopurine, Spectrochim. Acta Part A Mol Biomol Spectrosc. (2015) 204–213.
[33] D.H. Pereira, F.A. La Porta, R.T. Santiago, D.R. Garcia, T.C. Ramalho, New perspectives on the role of frontier molecular orbitals in the study of chemical reactivity: a review, Rev Virtual Quim (2016) 425–453.
[34] K. Fukui, Role of frontier orbitals in chemical reactions, Science 80 (1982).
[35] I.B. Obot, D.D. Macdonald, Z.M. Gasem, Density functional theory (DFT) as a powerful tool for designing new organic corrosion inhibitors: Part 1: an overview, Corrosion Sci. (2015) 1–30.

[36] T. Koopmans, Über die Zuordnung von Wellenfunktionen und Eigenwerten zu den Einzelnen Elektronen Eines Atoms, Physica (1934) 104–113.
[37] R.G. Parr, R.A. Donnelly, M. Levy, W.E. Palke, Electronegativity: the density functional viewpoint, J. Chem. Phys. (1978) 3801–3807.
[38] R.G. Parr, R.G. Pearson, Absolute hardness: companion parameter to absolute electronegativity, J. Am. Chem. Soc. (1983) 7512–7516.
[39] R.G. Parr, Chattaraj PK. Principle of maximum hardness, J. Am. Chem. Soc. (1991) 256–258.
[40] H. Chermette, Chemical reactivity indexes in density functional theory, J. Comput. Chem. (1999) 129–154.
[41] L.H. Mendoza-Huizar, C.H. Rios-Reyes, Chemical reactivity of Atrazine employing the Fukui function, J Mex Chem Soc (2011) 142–147.
[42] J.F. Janak, Proof that ∂E∂ni=ε in density-functional theory, Phys. Rev. B (1978) 165–168.
[43] L. Von Szentpály, Studies on electronegativity equalization. Part 1. Consistent diatomic partial charges, J Mol Struct THEOCHEM (1991) 71–81.
[44] W. Yang, R.G. Parr, Hardness, softness, and the fukui function in the electronic theory of metals and catalysis, Proc. Natl. Acad. Sci. U. S. A. (1985) 4049–4050.
[45] R.G. Parr, L.V. Szentpály, S. Liu, Electrophilicity index, J. Am. Chem. Soc. (1999) 1922–1924.
[46] P.K. Chattaraj, U. Sarkar, Theoretical Aspects of Chemical Reactivity, 2007, pp. 269–286.
[47] C. Morell, A. Grand, A. Toro-Labbé, New dual descriptor for chemical reactivity, J. Phys. Chem. (2005) 205–212.
[48] J. Padmanabhan, R. Parthasarathi, M. Elango, et al., Multiphilic descriptor for chemical reactivity and selectivity, J. Phys. Chem. (2007) 9130–9138.
[49] M.A. Spackman, D. Jayatilaka, Hirshfeld surface analysis, CrystEngComm (2009) 19–32.
[50] A. Uppal, P. Kour, A. Kumar, Y. Khajuria, Synthesis, structural, vibrational, electronic, thermal and Fukui analysis of diethyl (hydroxy(4-methoxyphenyl) methyl) phosphonate, J. Mol. Struct. (2018) 218–227.
[51] A.R. Allouche, Gabedit - a graphical user interface for computational chemistry softwares, J. Comput. Chem. 32 (2010) 174–182.
[52] K. Momma, F. Izumi, VESTA 3 for three-dimensional visualization of crystal, volumetric and morphology data, J. Appl. Crystallogr. 44 (6) (2011) 1272–1276.
[53] T. Lu, F. Chen, Multiwfn: a multifunctional wavefunction analyzer, J. Comput. Chem. 33 (5) (2012) 580–592.
[54] N. Kosar, K. Shehzadi, K. Ayub, T. Mahmood, Theoretical study on novel superalkali doped graphdiyne complexes: unique approach for the enhancement of electronic and nonlinear optical response, J. Mol. Graph. Model. 97 (2020) 107573.
[55] H. Sajid, K. Ayub, T. Mahmood, Exceptionally high NLO response and deep ultraviolet transparency of superalkali doped macrocyclic oligofuran rings, New J. Chem. 44 (2020) 2609–2618.
[56] H. Iikura, T. Tsuneda, T. Yanai, K. Hirao, A long-range correction scheme for generalized-gradient-approximation exchange functionals, J. Chem. Phys. 115 (2001) 3540–3544.
[57] J. Da Chai, M. Head-Gordon, Long-range corrected hybrid density functionals with damped atom-atom dispersion corrections, Phys. Chem. Chem. Phys. 10 (2008) 6615–6620.
[58] S. Dutta, P.S. Kharkar, N.U. Sahu, A. Khanna, Molecular docking prediction and in vitro studies elucidate anti-cancer activity of phytoestrogens, Life Sci. 185 (2017) 73–84.
[59] Y. Fu, S.Q. Zhang, Y.X. Liu, et al., Design, synthesis, SAR and molecular docking of novel green niacin-triketone HPPD inhibitor, Ind. Crop. Prod. (2019) 566–575.
[60] O. Trott, A.J. Olson, Autodock vina, J. Comput. Chem. (2010) 455–461.
[61] F. Pavão, M.S. Castilho, M.T. Pupo, et al., Structure of Trypanosoma cruzi glycosomal glyceraldehyde-3-phosphate dehydrogenase complexed with chalepin, a natural product inhibitor, at 1.95 AÅ resolution, FEBS Lett. 520 (1–3) (2002) 13–17.
[62] D. Yusuf, A.M. Davis, G.J. Kleywegt, S. Schmitt, An alternative method for the evaluation of docking performance: RSR vs RMSD, J. Chem. Inf. Model. 48 (7) (2008) 1411–1422.
[63] T. Gaillard, Evaluation of AutoDock and AutoDock vina on the CASF-2013 benchmark, J. Chem. Inf. Model. 58 (8) (2018) 1697–1706.
[64] P. Borowiecki, A.M. Wawro, P. Wińska, M. Wielechowska, M. Bretner, Synthesis of novel chiral TBBt derivatives with hydroxyl moiety. Studies on inhibition of human protein kinase CK2α and cytotoxicity properties, Eur. J. Med. Chem. (2014) 364–374.
[65] D.S. Biovia, H.M. Berman, J. Westbrook, et al., Dassault systèmes BIOVIA, discovery Studio visualizer, v.17.2, san diego: dassault systèmes, J. Chem. Phys. (2016) 21–9991.
[66] P.H. Yeh, Y.D. Shieh, L.C. Hsu, et al., Naturally occurring cytotoxic [3′→8″]-biflavonoids from podocarpus nakaii, J Tradit Complement Med 2 (3) (2012) 220–226.
[67] V. Arjunan, S. Mohan, Fourier transform infrared and FT-Raman spectra, assignment, ab initio, DFT and normal co-ordinate analysis of 2-chloro-4-methylaniline and 2-chloro-6-methylaniline, Spectrochim. Acta Part A Mol Biomol Spectrosc 72 (2) (2009) 436–444.
[68] D. Zeroka, J.O. Jensen, A.C. Samuels, Infrared spectra of some isotopomers of ethylamine and the ethylammonium ion: a theoretical study, J Mol Struct THEOCHEM 465 (1999) 119–139.
[69] A.O. Zacharias, A. Varghese, K.B. Akshaya, M.S. Savitha, L. George, DFT, spectroscopic studies, NBO, NLO and Fukui functional analysis of 1-(1-(2,4-difluorophenyl)-2-(1H-1,2,4-triazol-1-yl)ethylidene) thiosemicarbazide, J. Mol. Struct. (2018) 1–13.
[70] R.G. Pearson, Hard and soft acids and bases-the evolution of a chemical concept, Coord. Chem. Rev. (1990) 403–425.
[71] R. Huey, G.M. Morris, A.J. Olson, D.S. Goodsell, Software news and update a semiempirical free energy force field with charge-based desolvation, J. Comput. Chem. 28 (6) (2007) 1145–1152.
[72] L.A.A. Avelar, C.D. Camilo, S. De Albuquerque, et al., Molecular design, synthesis and trypanocidal activity of dipeptidyl nitriles as cruzain inhibitors, PLoS Neglected Trop. Dis. 9 (7) (2015), e0003916.